AIAA

AIAA 98-0960

Design of Three-Dimensional Hypersonic Inlets with Rectangular to Elliptical Shape Transition

M. K. Smart
National Research Council
Hypersonic Airbreathing Propulsion Branch
NASA Langley Research Center
Hampton, VA.

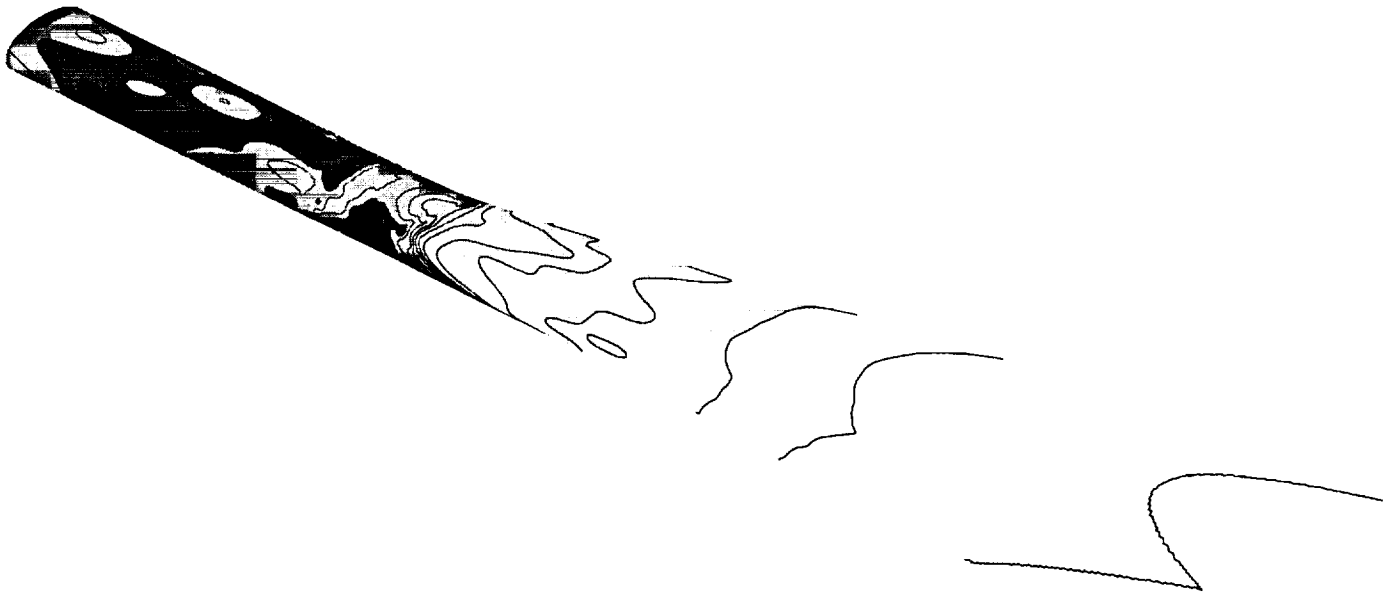

36th Aerospace Sciences Meeting & Exhibit
January 12–15, 1998 / Reno, NV

Design of Three-Dimensional Hypersonic Inlets with Rectangular to Elliptical Shape Transition

M. K. Smart
NASA Langley Research Center, Hampton, Virginia, 23681.

Abstract

A methodology has been devised for the design of three-dimensional hypersonic inlets which include a rectangular to elliptical shape transition. This methodology makes extensive use of inviscid streamtracing techniques to generate a smooth shape transition from a rectangular-like capture to an elliptical throat. Highly swept leading edges and a significantly notched cowl enable use of these inlets in fixed geometry configurations. The design procedure includes a three-dimensional displacement thickness calculation and uses established correlations to check for boundary layer separation due to shock wave interactions. Complete details of the design procedure are presented and the characteristics of a modular inlet with rectangular to elliptical shape transition and a design point of Mach 7.1 are examined. Comparison with a classical two-dimensional inlet optimized for maximum total pressure recovery indicates that this three-dimensional inlet demonstrates good performance even well below its design point.

Nomenclature

C_f	skin friction
CRI	internal contraction ratio of inlet
CRT	total contraction ratio of inlet
h_1,h_2	metrics of surface streamlines
K_1,K_2	curvatures of surface streamlines
H	total enthalpy
L	distance from throat to exit
m	mass flow
m_C	mass capture percentage = m_{ca}/m_{ex}
M	Mach number
P	pressure
P_R	inlet compression ratio = P_{ex}/P_∞
P_T	total pressure recovery
q	dynamic pressure
Re	Reynolds number
R_0	radius of axisymmetric compression field capture
s	distance along streamline
T	temperature
T_R	inlet temperature ratio = T_{ex}/T_∞
u,v,w	velocity components
x,y,z	coordinate directions
α	parameter in lofting procedure
β	boundary layer cross flow angle
δ	boundary layer thickness
δ^*	boundary layer displacement thickness
η_{KD}	process efficiency
η_{KE}	kinetic energy efficiency
γ	ratio of specific heats
ρ	density
μ	viscosity
θ	flow turning

Subscripts

B	bow shock
c	combustor
ca	inlet capture
cb	center-body
cc	cowl closure
e	boundary layer edge
ex	exit
I	incipient separation
inv	inviscid
vis	viscous
∞	freestream
δ	boundary layer thickness

Introduction

The design of efficient inlets for hypersonic vehicles utilizing airframe integrated scramjet modules is a subject of interest at NASA Langley Research Center. In these configurations the vehicle bow shock performs the initial compression, and the capture shape for the inlet of each scramjet module is required to form three sides of a rectangle so that the modules may be mounted side-by-side. Other requirements are that inlets have good starting characteristics at ramjet/scramjet take-over speeds (Mach 4-5), operate over a large Mach number range, and be efficient once the vehicle has accelerated to its cruise condition. To reduce structural complexity there is also a strong preference for an inlet with fixed geometry and no requirement for boundary layer bleed. A further desirable inlet feature for some scramjet applications is a cross-sectional shape transition from the rectangular-like

---

*National Research Council Research Associate, Hypersonic Airbreathing Propulsion Branch, Mail Stop 168, Member AIAA.

capture to an elliptical throat. The inlet may then be used in combination with an elliptical combustor, which is superior to a rectangular combustor in terms of the structural weight required to contain a specified pressure and the wetted surface area needed to enclose a specified cross-sectional area. Fluid dynamic problems associated with hypersonic corner flows are also avoided with this type of configuration. The aforementioned inlet characteristics constitute a set of stringent requirements, some of which will not be able to be met in a practical vehicle. Hypersonic inlets designed using fully three-dimensional design methodologies may be able to satisfy many of these demands.

A number of three-dimensionally curved missile inlets with circular or elliptical throats were designed and tested in the 1960's by Hartill[1], Kiersey and Snow[2] and Kutshenreuter[3]. These fixed geometry inlets showed good performance in the wind tunnel and self started at internal contraction ratio's well above the one-dimensional inviscid starting limit determined by Kantrowitz[4]. However the performance of these inlets was difficult to predict with the computational tools available at that time. In the mid 1980's Simmons and Wiedner[5] produced a thorough literature review of three-dimensional hypersonic inlet design and described a conceptual design methodology for inlets with rectangular capture and circular throat. This methodology was an adaption of the 1960's design procedures to modular scramjet configurations, and comprised of a streamtracing technique in combination with a lofting procedure for cross-sectional shape transition. No detailed design and testing of inlet configurations was performed as a result of this study. An interesting article by Billig[6] described the design and wind tunnel testing of a scramjet missile concept at APL/JHU between 1962 and 1978. This missile included a three-dimensionally curved inlet based on tracing streamlines through a Busemann inlet flowfield, and was similar to that described in Ref. 2.

The aim of a current project at NASA Langley is the development of a detailed design methodology for three-dimensional hypersonic inlets. This project has been undertaken to examine the possible advantages of three-dimensional inlet geometries relative to more traditional inlets based on essentially two-dimensional design methodologies. Extensive use of three-dimensional computational tools is required for this work and the methodology utilizes many of the ideas developed in the aforementioned inlet studies[1-3,5]. Some preliminary work on this project involving the design of streamtraced hypersonic inlets was presented in Smart[7]. The current article is an extension of this work to hypersonic inlets in which the shape of the inlet capture and throat are specified a priori, something not able to be accomplished using streamtracing techniques alone. In particular, the work concentrates on inlets with rectangular to elliptical shape transition (REST). The constraints placed on the inlets designed in this work are that they must be suitable for modular scramjet applications, have fixed geometry, be able to self start at Mach 4-5, and not contain large boundary layer separations. Complete details of the design methodology are presented and the characteristics of a REST inlet with a design point of Mach 7.1 are examined.

REST Inlet Design Methodology

General Remarks

While computational methods and computer speed have improved markedly in the past 10 years, full Navier-Stokes calculations of turbulent three-dimensional hypersonic inlet flows are not a practical design tool at the present time. In the current work the inlet design methodology utilizes three-dimensional inviscid calculations to determine the shock structure and surface pressure signature of inlet shapes. This information is then compared with empirical correlations to check for boundary layer separations caused by shock wave interactions. If no boundary layer separation is apparent, then a three-dimensional boundary layer calculation is performed in order to determine the physical inlet shape which generates the inviscid flowfield. With the use of current super computers the cycle time for this process can be reduced to the point where numerous design iterations can be performed in a relatively short period.

The complete design procedure may be logically separated into two sections; (i) determination of the invsicid inlet shape; and (ii) calculation of the viscous correction. The inviscid portion of the design procedure is summarized in this section. A description of the technique used to calculate the three-dimensional viscous correction to the inviscid shape is included later. While the inviscid inlet shapes generated using this methodology do not coincide with the streamlines through any known flowfield; i.e. they cannot be called "streamtraced inlets", streamtracing techniques form the basis of the inviscid portion of the design procedure. These will first be summarized, followed by a description of how streamtraced shapes may be combined to construct an inlet with a specified shape transition. The adaption of established shock wave/boundary layer separation criteria to the types of shock interactions that occur in REST inlets completes the inviscid portion of the design procedure.

Streamtraced Inlets

The streamtracing process provides a powerful but relatively simple technique for determining the inviscid shape of an inlet with pre-determined capture shape and pressure ratio. The general steps are as follows:

1. Calculate a desirable compressive flowfield which has the same pressure ratio as required for the inlet. In practice this flowfield is usually chosen to be either two-dimensional or axisymmetric, but it is not restricted to these.
2. Define a capture perimeter which fits within the entrance of the compression field.
3. Calculate the path of the streamlines which pass through the capture perimeter. The stream surface

defined by these streamlines constitutes the inviscid shape of the streamtraced inlet.

The key to the design of efficient streamtraced inlets is the choice of the compression field through which the streamlines are traced. Whatever features are contained in this flowfield will also be a part of the flowfield generated inside the inlet. The current choice for the form of this flow is an axisymmetric compression field with a constant radius center-body. This flowfield, a schematic of which is shown in Fig. 1, takes advantage of the isentropic compression inherent in axisymmetric compression fields, while the center body removes the flow region near the axis where shock focusing can lead to high losses. The compression field chosen for a particular inlet design is therefore defined by the shape of the outer surface containing the compression field, the center body radius and the entrance Mach number.

Once the compression field has been calculated, a multitude of possible capture perimeters are available to the inlet designer. The modular application of the current work requires that the capture shape have parallel sides and a straight top at right angles to the sides, however the bottom may be of more general shape. Typically the largest capture perimeter of the desired shape which fits within the annular entrance flow is chosen so as to minimize the inlet length/cross-sectional area ratio. Figure 1 shows the inlet formed by a rectangular capture shape. Note that streamlines passing through the capture shape perimeter remain straight up to the point each encounters the shock surface. Hence the surfaces of the inlet need not start until the streamlines reach the shock wave, allowing the side leading edges of the inlet to be highly swept and the bottom surface to be notched. It is these characteristics of the current design methodology which enable the inlet to operate well below its design point by spilling flow below its bottom surface.

An important step in the current inlet design process involves calculation of the outer surface profile of the axisymmetric compression field. This profile determines the character of the compression field (and in turn the quality of the inlet), which is a trade-off between maximum total

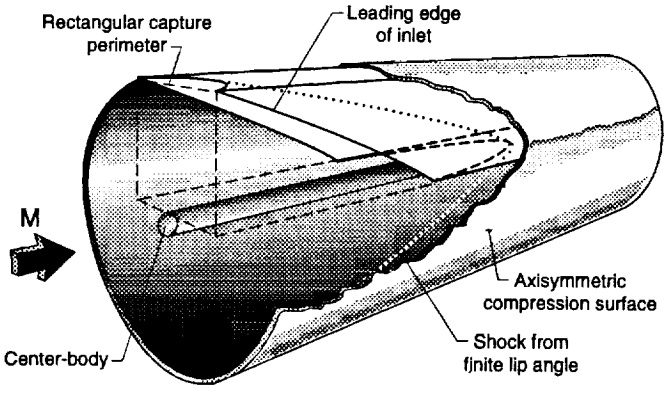

Figure 1. Schematic of a streamtraced inlet based on an axisymmetric compression field.

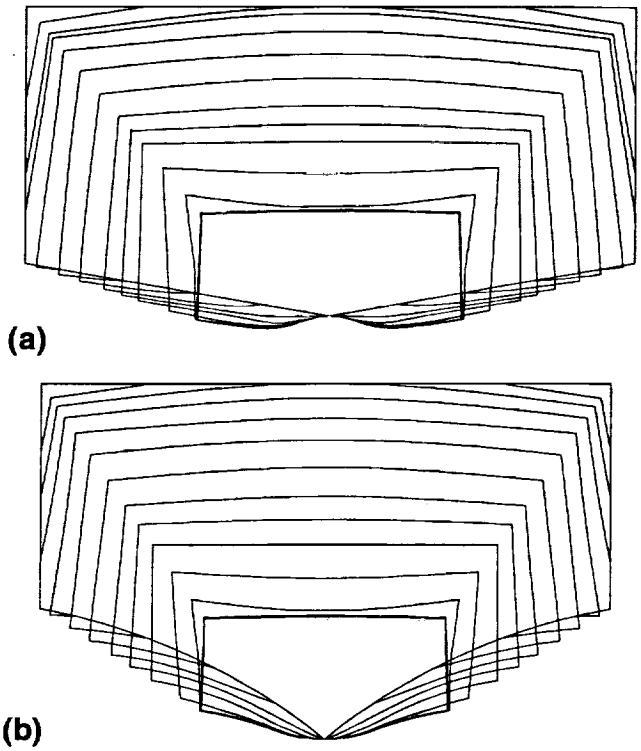

Figure 2. Inlet cross-section shape distributions for different capture perimeters.

pressure recovery, maximum shock strength that will not produce boundary layer separation, minimum drag and minimum exit flow non-uniformity. In the current work a preliminary profile is determined by reversing an axisymmetric expansion nozzle profile with center-body radius, throat Mach number and pressure ratio similar to the desired inlet. The profile is then shortened by converting the initial portion to a finite lip angle. Finally, some iteration of the expansion nozzle center-body radius and throat profile shape is performed so that significant canceling of the axisymmetric shock wave occurs at the profile throat. This process had been found to generate axisymmetric compression fields which are suitable for practical streamtraced inlet configurations.

In the current work the axisymmetric compression fields are calculated using the NASA Langley program, SEAGULL, which is an inviscid shock fitting code specifically designed for supersonic internal flows.[8] Once the axisymmetric compression field has been calculated, the paths of streamlines passing through the capture perimeter may be determined. In the current work the streamtracing routine built into the plotting program TECPLOT[9] was utilized. Figure 2(a) shows the distortion of a rectangular capture perimeter as the streamlines pass through a typical axisymmetric compression field used in the current work. Note that this capture shape leads to a convex bottom surface which is unacceptable for a practical inlet. A capture perimeter that generates a more suitable cross-sectional shape

distribution throughout the compression field is shown in Fig. 2(b). This capture shape still satisfies the modular requirements of the current work, but the curved bottom of the capture perimeter leads to a less distorted cross-section at the inlet throat. The inlet shape represented in Fig 2(b) typifies the basic streamtraced inlet shape that is adapted in the current work to allow independent specification of both capture and throat shapes.

Inlet Shape Transition

Streamline tracing techniques enable generation of an inlet shape which has almost identical characteristics to a pre-determined desirable flowfield, but an independently specified capture shape. Similarly, streamtracing techniques also enable determination of an inlet shape with characteristics almost identical to a pre-determined flowfield, but with an independently specified throat shape. This can be obtained by simply tracing streamlines backwards through the original flowfield. In the current methodology an inlet with an independently specified capture *and* throat shape is determined by combining a number of streamtraced shapes to produce a smooth transition from capture to throat. If this combination of streamtraced shapes is done in a judicious way, the resultant inlet shape can produce a flowfield with characteristics only slightly degraded relative to the original flowfield.

The particular interest of the current work is in the generation of inlets with transition from a rectangular-like capture shape to an elliptical throat (REST). The general steps used to perform this are as follows:

1. Calculate a desirable axisymmetric compression field which has the same pressure ratio as required by the inlet.
2. Generate a streamtraced inlet shape using a rectangular-like capture perimeter such as that shown in Fig. 2(b); this shape is designated shape A.
3. Generate a second streamtraced inlet shape using a capture perimeter similar to shape A, but with radiuses corners; this is designated shape B and a typical cross-sectional shape distribution for it is shown in Fig. 3(a).
4. Generate a third inlet shape, this time with an elliptical throat that has the same throat area as shape A; this is designated shape C and a typical cross-sectional shape distribution for it is shown in Fig. 3(b).
5. Smoothly combine all three inlet shapes to form a REST inlet which has the capture shape of A, the cross-sectional shape of B at cowl closure, and the same throat shape as C.

Smooth shape transition between the three streamtraced inlets is accomplished in the current work with a mathematical lofting procedure developed by Barger[10]. This procedure enables smooth transition from an initial to a final shape with a remaining free parameter that can be adjusted, in this

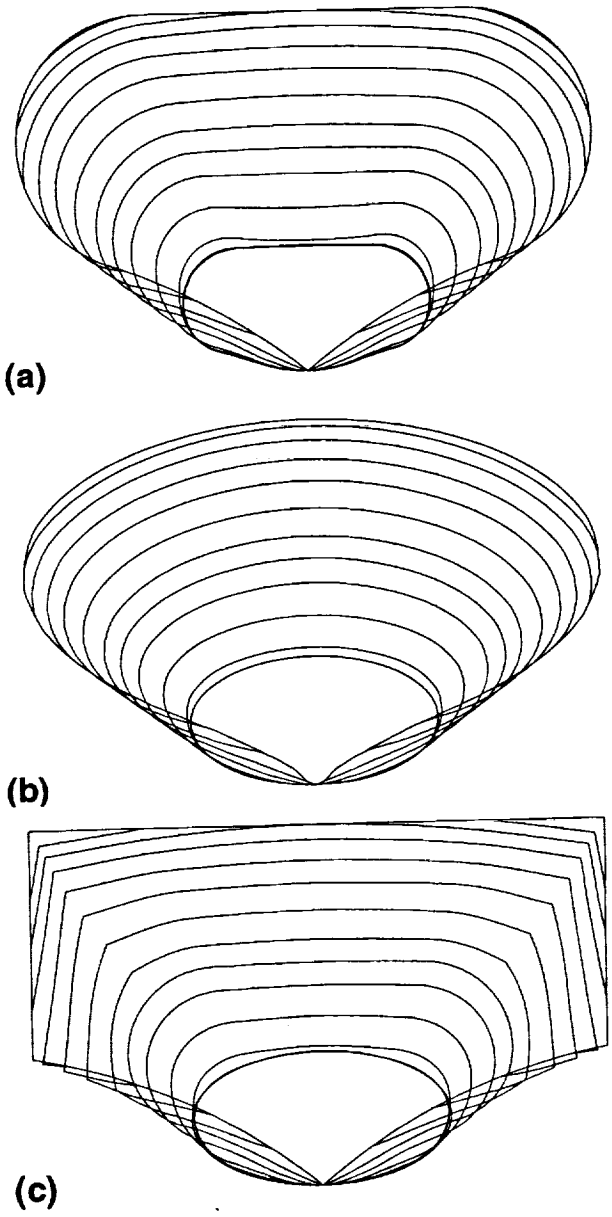

Figure 3. Cross-section shape distributions for different inlets.

instance, to optimize the REST inlet for maximum total pressure recovery or minimum exit flow non-uniformity. For example, if $f_1(y)$ and $f_2(y)$ represent the cross-sections of shape A and B at some intermediate station between inlet capture (x_{ca}) and cowl closure (x_{cc}), then the cross-section of the REST inlet at the intermediate station is given by:

$$f(y) = [f_1(y)]^{1-E(x)} [f_2(y)]^{E(x)} \qquad (1)$$

$$\text{Where} \quad E(x) = \left(\frac{x - x_{ca}}{x_{cc} - x_{ca}}\right)^{\alpha} \; ; \quad \alpha > 0$$

Combination of cross-sections in this way smooths out regions

of high curvature. Furthermore, if α is small, the intermediate shape is dominated by $f_2(y)$ except near x_{cc}; and if α is large, the intermediate shape is dominated by $f_1(y)$ except very close to x_{cc}. Values of $1.0 < \alpha > 5.0$ have been found to supply sensible shape transitions for the current application. Figure 3(c) shows a typical cross-sectional shape distribution for a REST inlet with $\alpha = 3.5$.

Once the coordinates of the REST inlet cross-sectional shapes are known, these are used to generate a computational grid for calculating the flowfield generated by the inlet. It is noted that while the on-design performance of a streamtraced inlet is already pre-determined as part of the design procedure, determination of the REST inlet on-design performance requires the use of fully three-dimensional computational methods.

Shock Wave/Boundary Layer Interactions

It is of considerable importance to include some treatment of shock wave/boundary layer interactions in the inviscid portion of the inlet design procedure. Shock induced boundary layer separation can produce significant losses within the inlet, and may cause inlet unstart. Large separated regions also invalidate the use of the boundary layer equations for calculating the viscous correction needed to determine the physical shape of the inlet. Established incipient separation criteria are adapted in the current work to determine the maximum shock strength allowable within the inlet. In practice it is the desire to inhibit boundary layer separation that usually sets a limit on the minimum length of an inlet.

Shock wave/boundary layer interactions are generally separated into two categories:

1. Two-dimensional interactions such as those that occur at a straight compression ramp or when a planar oblique shock reflects at a surface. These interactions, by definition, generate no crosswise or lateral turning of inviscid flow.
2. Swept interactions, such as the interaction produced by a planar oblique shock wave as it sweeps across a flat plate from a perpendicular fin. These interactions are inherently three-dimensional, but only involve turning of inviscid flow within planes parallel with the upstream surface (when separation does not occur).

Incipient separation criterion for turbulent boundary layers have been established for both these types of interactions, most notably by Korkegi[11]. These correlations indicate that swept interactions give rise to somewhat earlier separation than two-dimensional interactions. Korkegi[11] suggested that this is due to the fact that the surface streamlines are forced to undergo complete reversal in direction in the two-dimensional interaction, whereas surface streamlines in the swept interaction only undergo a small direction change associated with lifting off the surface along a swept back separation line.

The shock wave/boundary layer interactions that occur in the inlets designed using the current methodology do not belong to either category. These involve reflection of curved shocks at smoothly curved surfaces, where the line of reflection is generally swept back with respect to the on-coming flow. In a typical REST inlet the incident shock surface reflects at the crotch of the cowl, sweeps across the bottom and side surfaces and undergoes significant cancellation upon striking the top surface at the throat. While it is probably reasonable to treat the shock wave/boundary interaction on the top surface as approximately two-dimensional (i.e. put it in category 1), the interactions on both the bottom and side surfaces exhibit characteristics of both categories. Given this, an approximate procedure for predicting the incipient separation of "mixed" interactions has been developed.

Assuming for explanation purposes that flow is inviscid, the clear physical difference between the two shock interaction categories is the direction of flow turning relative to the upstream surface. Two dimensional interactions contain no flow deflection in the plane of the upstream surface, whereas swept interactions involve lateral deflection in the plane of the upstream surface only. A mixed interaction such as occurs at a swept ramp or in a REST inlet contains flow deflection both parallel and normal to the upstream surface. Inviscid flowfield solutions of REST inlets are determined as part of the current design procedure, hence the inviscid flow deflection through a shock interaction is known. Knowledge of the inviscid flowfield, together with the availability of different separation criterion for lateral and normal turning (categories 1 and 2 respectively), enables an estimate for the separation limit of a mixed interaction to be established by breaking the inviscid flow deflection into components normal and parallel to the upstream surface.

The incipient turbulent boundary layer separation criterion for swept interactions (category 2) proposed by Korkegi[11] is simply:

$$M\theta_i = 0.3 \quad (radians) \tag{2}$$

This criterion shows good correlation with experimental data up to Mach 6 for $Re_\delta > 10^5$. For standard swept interactions this criterion may be expressed in terms of pressure rise as $P_i/P = 1.50$. For mixed interactions the criterion must be left in terms of M and θ_i, as the relationship between the pressure rise and lateral flow deflection that occurs through the interaction depends on its mixed nature. Equation (2) then becomes a local criterion and can be calculated for each surface streamline in an inviscid flow calculation. In general the lateral flow deflection in a mixed interaction is associated with a larger pressure rise than flow deflection in an equivalent swept interaction, so mixed interactions separate at a higher pressure ratio than standard swept interactions.

The incipient turbulent boundary layer separation criterion for two dimensional interactions (category 1) proposed by Korkegi[11] is:

$$P_i/P = 1.0 + 0.3M^2 \qquad M < 4.5 \qquad (3a)$$

$$P_i/P = 0.17M^{2.5} \qquad M \geq 4.5 \qquad (3b)$$

This criterion shows good correlation with experimental data up to Mach 8 for $Re_\delta > 10^5$. The two-dimensional interaction is the least likely of any interaction type to be separated by an imposed pressure rise, hence equation (3) defines an upper limit for all interactions. Mixed interactions with sweep lines nearly normal to the on-coming flow generate little lateral flow deflection, so the swept separation criterion of equation (2) may not be accurate. Equation (3) supplies a maximum upper limit on the pressure rise a mixed interaction can withstand, regardless of the magnitude of its lateral flow deflection.

Based on the aforementioned ideas, the following three step procedure for predicting incipient separation of mixed interactions is proposed:

1. Determine the lateral flow deflection through the interaction.
2. Check for separation using equation (2).
3. If separation is not predicted by equation (2), perform a further check against equation (3).

If neither equation (2) or (3) indicate separation, then the inlet boundary layer is expected to proceed smoothly through the interaction. This separation prediction procedure is included as part of the REST design test case described in the next section.

Inviscid Design of a Mach 7.1 Inlet

Design Parameters

The inviscid portion of the design methodology described in the previous section is applied in the current article to a scramjet inlet module mounted beneath a Mach 7.1 cruise vehicle. The vehicle is assumed to travel on a constant dynamic pressure trajectory of $q = 50kPa$. In combination with a 6° forebody compression, the inlet is required to supply

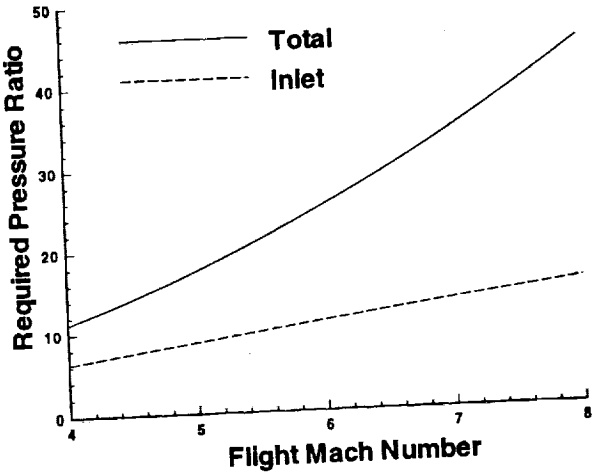

Figure 4. Required pressure ratio's for a Mach 7.1 inlet.

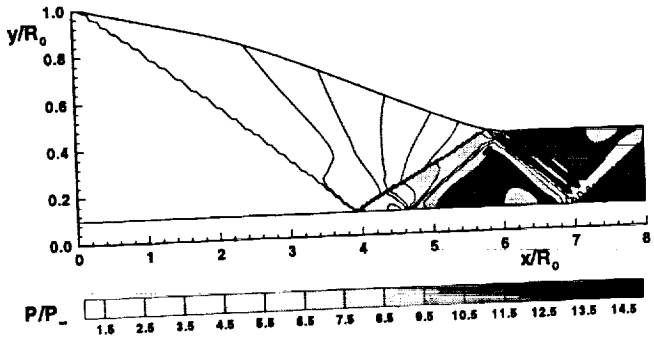

Figure 5. Axisymmetric compression field used to design the Mach 7.1 REST inlet.

the scramjet combustor with flow at a mean pressure of $P_c = 50kPa$. The inlet and overall pressure ratio's required in this instance for flight between Mach 4 and 8 are plotted in Fig. 4. At the Mach 7.1 design point, flow enters the inlet at M = 6.00 and the required inlet pressure ratio is $P_R = 13.50$. All calculations performed for the current article assume air flow at constant ratio of specific heats $\gamma = 1.4$.

Pressure contours in the axisymmetric compression field calculated for this case are shown in Fig. 5. In this instance a lip angle of 4° and a center-body radius of $r_{cb}/R_0 = 0.10$ were used. These values result from a compromise between minimum length and the requirement for no boundary layer separation. The throat profile and its position were chosen to perform the maximum amount of shock cancellation, leading to relatively uniform flow exiting the inlet. The properties of streamtraced inlets that are generated using this flowfield would be very close to those shown in Fig.5. The properties of a REST inlet constructed using this flowfield will depend on how the different streamtraced shapes are combined to form the required shape transition. After some iteration involving the geometry of the bottom edge of the capture perimeter, the radii of the corners at cowl closure, the aspect ratio of the throat, and the $\alpha's$ used in the lofting procedure, the REST inlet shown in Fig. 6 was generated. This iteration required the use of the fully three-dimensional computational methods described in the next sub-section. Note the significant sweep of both the side and top leading edges of the inlet capture, the extensive notch in the cowl and the transition from a capture shape with pronounced

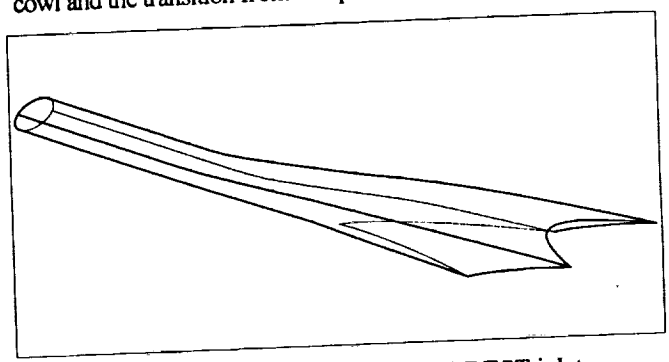

Figure 6. Pictorial view of the Mach 7.1 REST inlet.

corners to a throat with elliptical cross-section. The quick transition to a rounded shape immediately after capture minimizes hypersonic corner flow problems. The overall contraction ratio for this inlet is $CRT_{INV} = 5.92$, with an internal contraction ratio of $CRI_{INV} = 2.34$. This inlet shape is typical of those obtained using the current design methodology.

Three-Dimensional Inviscid Flow Calculations

The three dimensional inviscid flowfields generated by the inlet shown in Fig.6 have been calculated using the CFD code GASPv3.[12] This code utilizes cell centered, finite volume, upwind methods to solve the three dimensional, unsteady, compressible Euler equations. A mixed topology grid was found to be the most suitable for REST inlet calculations. This grid consisted of 545 planes normal to the freestream direction with each plane containing a central 37x37 H-type mesh constructed within a peripheral 17x109 C-type mesh as depicted in Fig. 7. This type of grid allowed for a smooth transition from the cornered entrance plane to the elliptical exit without unsatisfactory cell distortion. It can also be easily refined at the walls for any subsequent Navier-Stokes computations. Typical CPU times of 14 minutes were obtained on a Cray C-90 for space marching calculations with 4 orders of magnitude convergence. It was found that results were obtained most efficiently by space marching the solution with a first order scheme in the streamwise direction, and using a third order Roe flux difference splitting scheme incorporating a Spekreijse-Venkatakrishnan limiter to solve each plane. Use of higher order schemes in the marching direction led to oscillations behind the shock that could only be removed by performing a fully elliptic calculation. For the present calculations the inlet is assumed to be mounted underneath the vehicle and between identical modules. Flow spillage upstream of the notched cowl is modeled by using an extrapolation boundary condition for boundary cell faces ahead of the leading edge.

Inviscid flow field calculations have been performed at the Mach 7.1 design condition as well as at Mach 5.5 and 4.0. A comparison of the results of these calculations supplies some insight into the development of the inlet flow structure as the vehicle accelerates to cruise conditions. Figures 8(a), (b) and (c) show pressure contours in the symmetry plane of the inlet at Mach 4.0, 5.5 and 7.1 respectively (with the vertical scale magnified to aid visualization). At Mach 4.0 the inlet shows considerable spillage below the notched cowl and the cowl shock can be seen to strike the top surface well upstream of the throat. Minimal shock cancellation occurs in this instance and an extensive shock system can be seen downstream of the throat. At Mach 5.5 the shock waves in the flow are swept further downstream, leading to considerably less spillage than at Mach 4.0. Some shock cancellation does occur at the inlet throat, however significant flow non-uniformity persists at the inlet exit. At the Mach 7.1 design point the leading shock wave passes only slightly upstream of the cowl and the cowl shock is almost canceled at the throat. Minimal spillage occurs in this instance and the flow structure, while not being identical to the original compression field, is only slightly degraded in terms of exit flow non-uniformity and total pressure recovery. Given the significant shape transition of the inlet, reduction of flow degradation relative to the original compression field to the level observed here is considered to be a significant achievement.

Pictorial views of the on-design flowfield within the Mach 7.1 REST inlet are shown in Figs. 9(a) and (b). Figure 9(a) shows pressure contours on the surfaces of the inlet, while Fig. 9(b) shows pressure contours at a number of flow cross-sections along the inlet length. Note that upstream of cowl closure the shock wave generated by the inlet is almost axisymmetric, even though the inlet has corners. Also note that the top surface pressure distribution contains very little lateral variation upstream of the throat, indicating that it does not see any swept shock waves. Swept shock wave/boundary layer interactions involving the top surface boundary layer (which has been ingested from the forebody) are a considerable problem in side wall compression inlets[13]. In the current configuration only the side and bottom inlet surfaces encounter swept shock waves. These interactions have a less significant effect on the overall performance of the inlet as the boundary layer thickness is considerable less than on the top surface. Checks for boundary layer separation have been made for the shock wave/boundary layer interactions associated with this flowfield using the procedure outlined in the previous section. These indicated that the swept interaction on the bottom surface may induce some level of separation, while interactions on the top and side surfaces are below the incipient separation limit. Boundary layer separation on the bottom of the inlet generates a weak vortical structure that will be swept across the bottom and side surfaces as it flows downstream. This type of separation, involving the thin bottom surface boundary layer, is not considered to pose a significant problem for practical inlet operation.

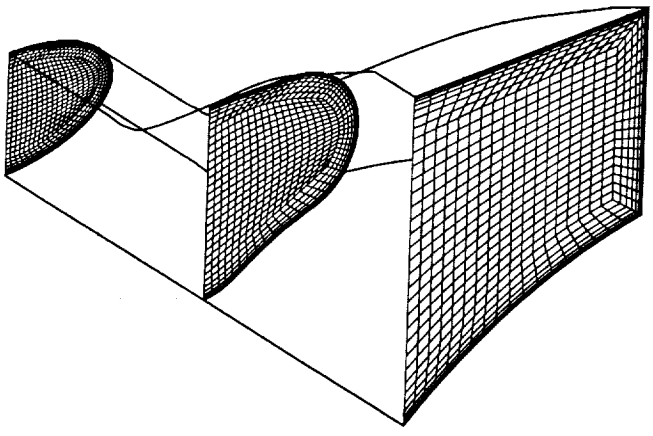

Figure 7. Schematic of the grid used for computations.

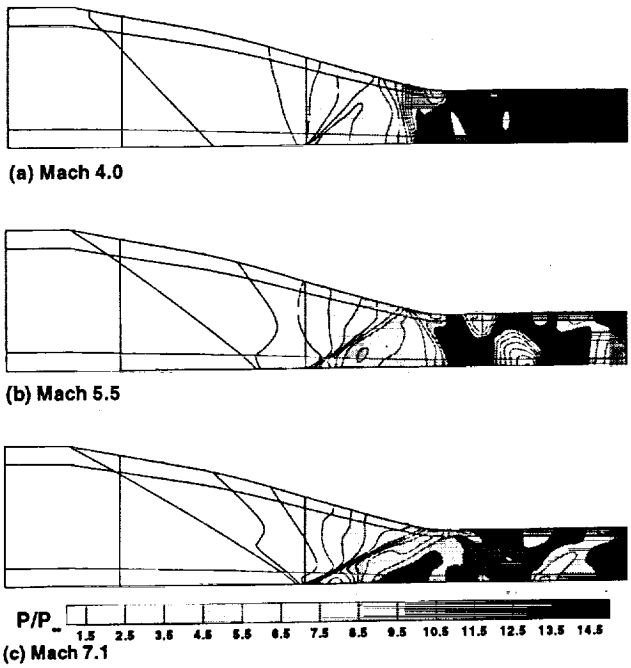

Figure 8. Symmetry plane pressure contours in the Mach 7.1 REST inlet.

Table 1 lists some mass flow weighted properties of the inlet flowfield at x/R_0 = 8.0, including mass capture percentage (m_C), compression ratio (P_R), temperature ratio (T_R) and exit Mach number (M_{ex}). These properties were calculated by converting the non-uniform flowfield at x/R_0 = 8.0 to an equivalent one-dimensional flow with the same total enthalpy, stream thrust, area and mass flow. The listed property variations correspond to half the maximum property range about the equivalent one-dimensional value. It is interesting to note that the pressure rise generated by the fixed geometry REST inlet remains relatively constant even well below its design point. This would allow a flight vehicle to accelerate along a reduced dynamic pressure trajectory if desired. Also of interest is the Mach 4.0 mass capture of 84.4%, meaning that less than 16% of the mass flow compressed by the inlet is wasted. Of the three Mach numbers examined, exit flow non-uniformity is greatest for the Mach 5.5 case. Although the Mach 4.0 case is farthest from the design point, the greater wave angles associated with the lower Mach number flow produce considerable wave cancellation to occur by x/R_0 = 8.0.

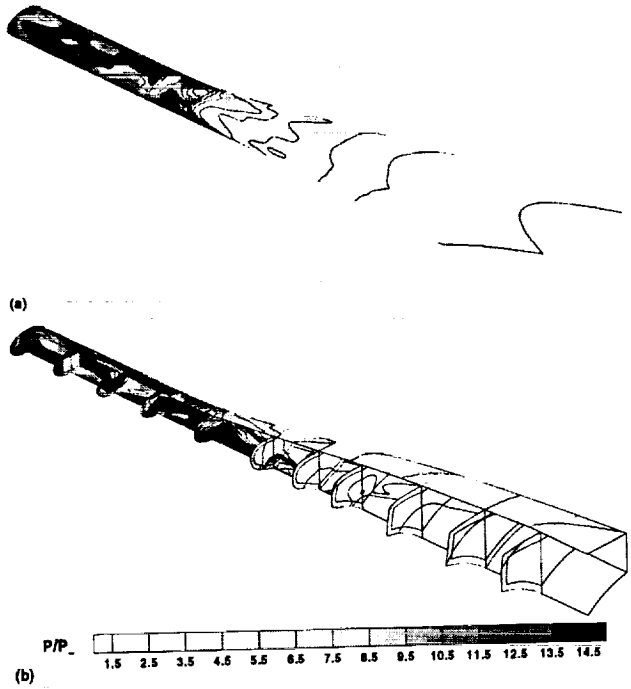

Figure 9. Pictorial views of the on-design Mach 7.1 REST inlet flowfield.

	Mach 4.0	Mach 5.5	Mach 7.1
m_C	84.4%	94.0%	99.6%
P_R	14.7 +/- 3.0%	13.8 +/- 19.1%	13.6 +/- 9.8%
T_R	2.18 +/- 2.2%	2.15 +/- 5.8%	2.14 +/- 6.4%
M_{ex}	1.77 +/- 2.7%	2.83 +/- 5.3%	3.76 +/- 4.2%

Table 1 - Mach 7.1 REST inlet characteristics.

Comparison with a two-dimensional Inlet

In order to gauge the effectiveness of the current REST inlet its performance can be compared with a classical two-dimensional inlet optimized for maximum total pressure recovery. Figure 10 shows a schematic of the 2-D, 3 shock inlet configuration used for comparison, which is assumed to have shock angles optimized for maximum total pressure recovery and perfect shock reflection. Performance properties for the REST inlet (including the forebody shock) are listed in Table 2. These may be directly compared with the performance parameters for a 2-D inlet that generates the same pressure rise at the same Mach number, listed in Table 3. It would appear that the REST inlet has better performance than the 2-D inlet in terms of total pressure recovery (P_T), Kinetic Energy Efficiency (η_{KE}) and Process Efficiency (η_{KD}) even well below its design point. This is a satisfying result as a 2-D, 3 shock inlet optimized in this way is generally

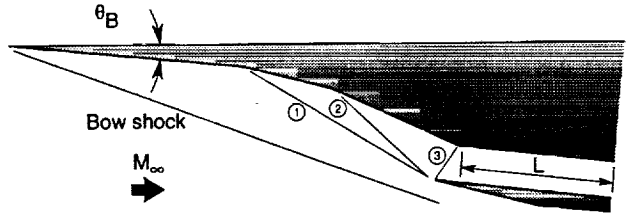

Figure 10. Schematic of the 2-D inlet used for performance comparison.

considered to have good performance. It important to note, however, that the values listed in Tables 2 & 3 are only based on inviscid calculations and do represent actual performance levels.

	Mach 4.0	Mach 5.5	Mach 7.1
P_T	0.944	0.900	0.867
η_{KE}	0.995	0.995	0.996
η_{KD}	0.990	0.982	0.978

Table 2 - REST inlet performance parameters.

	Mach 4.0	Mach 5.5	Mach 7.1
P_T	0.769	0.759	0.726
η_{KE}	0.976	0.986	0.991
η_{KD}	0.955	0.956	0.953

Table 3 - Two-dimensional inlet performance parameters.

Viscous Correction Calculations

General Remarks

The final stage of the design procedure involves calculation of a viscous correction to the inlet shape. Without enlargement of the inlet to allow for boundary layer growth, the overall pressure ratio generated during actual operation will be considerably higher than that predicted with the inviscid calculations. In the current work involving three-dimensionally curved inlets, the viscous correction is required to include some treatment of three-dimensional effects. However, full calculation of the corner flows at the entrance to the inlet or the shock wave/boundary interactions that occur throughout the inlet flowfield is not practical or desirable within a design procedure. In this instance we simply wish to obtain a smooth correction to the inlet shape such that the actual inlet flowfield contains a core region which is similar to that predicted with the inviscid calculations. Consequently, the viscous correction performed in the current work neglects corner flows, smooths any abrupt changes in the boundary layer displacement thickness due to shock interactions, and makes general use of the assumption that flow direction within the boundary layer does not vary greatly from the local inviscid flow direction. The corners are quickly smoothed out in a REST inlet, so the decision not to specifically model corner flows does not degrade the accuracy of the viscous correction. Furthermore, smoothing the abrupt displacement thickness change that occurs at shock interactions is a necessity for the design of any practical hypersonic inlet. Finally, the assumption of small cross flow is considered to be reasonable for hypersonic REST inlets, except in the local region surrounding shock wave interactions (with the usual caveat for large separations). As the details of the shock interaction region are smoothed out as part of the general viscous correction procedure, this deficiency is not significant.

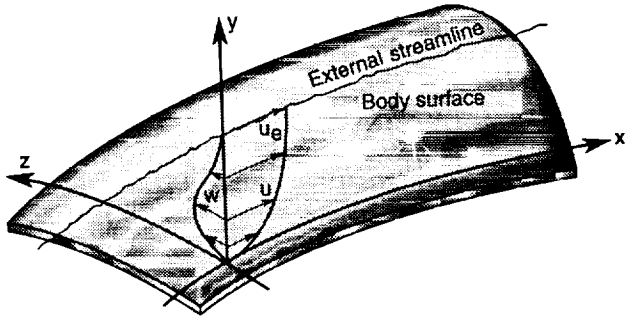

Figure 11. Streamline based coordinate system.

Small Cross Flow Equations

Two useful concepts for the study of three-dimensional turbulent boundary layers are streamline based orthogonal coordinate systems and the analogy between the axisymmetric and small cross flow boundary layer equations. Figure 11 shows a representation of a boundary layer on a curved surface where the x coordinate curves are formed by the projection of the external streamline onto the surface, the z coordinate curves remain on the surface and are orthogonal to the x curves, and the y coordinate is always normal to the surface. When using this system of coordinates, the u velocity component is called the streamwise velocity and the w velocity component is called the cross flow. In general, flow in the boundary layer differs from the inviscid freestream by the cross flow angle $\beta = \tan^{-1}(w/u)$. In many high speed flows where separation does not occur, β is everywhere small and the small cross flow assumptions may be used to simplify the full three-dimensional boundary layer equations. These assumptions are:

1. $w \ll u$
2. Cross flow derivatives, $\partial/\partial z$, are small compared to other terms in the governing equations.

Neglecting higher order terms in w and $\partial/\partial z$, the three-dimensional boundary layer equations for turbulent compressible flow can be shown to reduce to:

$$\frac{1}{h_1 h_2}\frac{\partial}{\partial x}(\rho u h_2) + \frac{\partial}{\partial y}(\overline{\rho v}) = 0 \qquad (4)$$

$$\frac{\rho u}{h_1}\frac{\partial u}{\partial x} + \overline{\rho v}\frac{\partial u}{\partial y} =$$

$$-\frac{1}{h_1}\frac{\partial P}{\partial x} + \frac{\partial}{\partial y}\left(\mu\frac{\partial u}{\partial y} - \rho\overline{u'v'}\right) \qquad (5)$$

$$\frac{\rho u}{h_1}\frac{\partial w}{\partial x} + \overline{\rho v}\frac{\partial w}{\partial y} - \rho u w K_2 + \rho u^2 K_1 =$$

$$-\frac{1}{h_2}\frac{\partial P}{\partial z} + \frac{\partial}{\partial y}(\mu\frac{\partial w}{\partial y} - \rho\overline{w'v'}) \quad (6)$$

$$\frac{\rho u}{h_1}\frac{\partial H}{\partial x} + \overline{\rho v}\frac{\partial H}{\partial y} =$$

$$-\frac{\partial}{\partial y}[k\frac{\partial T}{\partial y} - c_p\rho\overline{T'v'} + u(\mu\frac{\partial u}{\partial y} - \rho\overline{u'v'})] \quad (7)$$

In equations (4)-(7), h_1 and h_2 are the metric coefficients of the surface streamlines (which are functions of x and z only) and K_1 and K_2 are their streamwise and lateral curvatures, defined by:

$$K_1 = -\frac{1}{h_1 h_2}\frac{\partial h_1}{\partial z} \quad ; \quad K_2 = -\frac{1}{h_1 h_2}\frac{\partial h_2}{\partial x}$$

It is important to note that the cross flow velocity ( ) only appears in the cross flow momentum equation (equation (6)). Consequently the continuity, streamwise momentum and energy equations are decoupled from the cross flow and may be solved independently. Noting that $1/h_1\,\partial/\partial x = \partial/\partial s$ (where s is the distance along the streamline), equations (4), (5) and (7) become:

$$\frac{1}{h_2}\frac{\partial}{\partial s}(\rho u h_2) + \frac{\partial}{\partial y}(\overline{\rho v}) = 0 \quad (8)$$

$$\rho u\frac{\partial u}{\partial s} + \overline{\rho v}\frac{\partial u}{\partial y} =$$

$$-\frac{\partial P}{\partial s} + \frac{\partial}{\partial y}(\mu\frac{\partial u}{\partial y} - \rho\overline{u'v'}) \quad (9)$$

$$\rho u\frac{\partial H}{\partial s} + \overline{\rho v}\frac{\partial H}{\partial y} =$$

$$-\frac{\partial}{\partial y}[k\frac{\partial T}{\partial y} - c_p\rho\overline{T'v'} + u(\mu\frac{\partial u}{\partial y} - \rho\overline{u'v'})] \quad (10)$$

Equations (8)-(10) are analogous to the turbulent, compressible, axisymmetric boundary layer equations with h_2 in place of the radius of the axisymmetric body. Interestingly, neither of the curvature terms appear in the equations, indicating that streamline curvature has only a second order effect on the boundary layer in this instance. It is also important to underscore the physical significance of h_2. Simply stated, if $\partial h_2/\partial s > 0$, then streamlines diverge; if h_2 is constant, then streamlines are parallel and the flow is locally two-dimensional; and if $\partial h_2/\partial s < 0$, then streamlines converge. The inlet flowfields of interest in the current work include substantial variations in h_2, hence use of a two-dimensional boundary layer calculation would results in a poor estimate of the inlet boundary layer.

Given the geometrical properties of the inviscid streamlines and a closure model for the turbulent terms, equations (8)-(10) may be solved along each streamline using a space marching finite difference boundary layer code. If desired, the cross flow momentum equation can be subsequently solved along each streamline in order to calculate the cross flow velocity distribution. It is noted that both curvature terms will effect the cross flow velocity. Solution of the cross flow momentum equation was not attempted in the current work.

Finite Difference Calculations

The finite difference boundary layer code described in the book by Cebeci and Bradshaw[13] was adapted in the current work for non-isentropic edge conditions. This code uses an implicit iterative method due to Keller[14] to solve the transformed mass, momentum and energy equations for two-dimensional boundary layers. Solution of the axisymmetric boundary layer equations, or in our case, the small cross flow equations, was obtained by incorporating the Mangler transformation into the standard Levy-Lees transformation used in the code. A simply eddy-viscosity turbulence model due to Cebeci and Smith[15] was utilized. In this model a two layer formulation is used for the eddy viscosity and transition from laminar to turbulent flow is calculated using an intermitancy factor. The position at which transition begins must be supplied as input to the code.

In the unmodified code, the full edge conditions are input at the starting station, whereas the edge conditions in the remainder of the calculation are determined within the code using the imposed pressure distribution and the assumption of isentropic flow. In the current work the code was modified to read in both the pressure and velocity at the boundary layer edge along the full length of the calculation. Furthermore, the standard substitution of $\rho_e u_e \partial u_e/\partial s$ for the $-\partial P_e/\partial s$ term in the streamwise momentum equation was by-passed. These necessary changes required some small additions to the standard code, however its overall computational structure remained unchanged.

Viscous Correction to the Mach7.1 REST Inlet

The Mach 7.1 REST inlet described in this article is to be tested at its design point in a Mach 6 blow down wind tunnel at NASA Langley (Mach 7.1 flight corresponds to Mach 6.0 entering the inlet). An inlet model with a capture width of 152 mm is planned and typical freestream tunnel conditions for the tests are $M_\infty = 6.02$, $P_\infty = 2032\,Pa$ and $T_\infty = 63\,K$, which correspond to $Re_\infty = 2.6\times10^7/m$. The tunnel may be run for up to five minutes at these conditions, hence the viscous correction used to design the inlet model was calculated assuming adiabatic wall conditions. It is intended to trip the boundary layer approximately 12 mm downstream of the inlet

leading edges. Some results of the boundary layer calculations performed for this viscous correction are described in the following paragraphs.

The inviscid calculations of the Mach 7.1 REST inlet flowfield are used to determine the paths of streamlines used for boundary layer calculations. Unfortunately, the tangency boundary condition used by the CFD code GASPv3 causes an anomalous entropy layer to form at the wall downstream of shock/surface interactions. This defect becomes obvious in Euler calculations, and is typical of modern CFD codes written specifically for solution of the Navier-Stokes equations. The extent of the flow area contaminated by this error can be minimized by grid clustering near walls, but can only be removed by using a more complicated tangency boundary condition formulation. To mitigate the errors associated with the aforementioned anomalous entropy layer, significant grid clustering is employed (see Fig. 7) and flow properties from the 7th node away from the wall were superimposed on adjacent wall nodes. Streamlines were then traced in the boundary surfaces of the inlet grid using the TECPLOT[9] streamtracing routine.

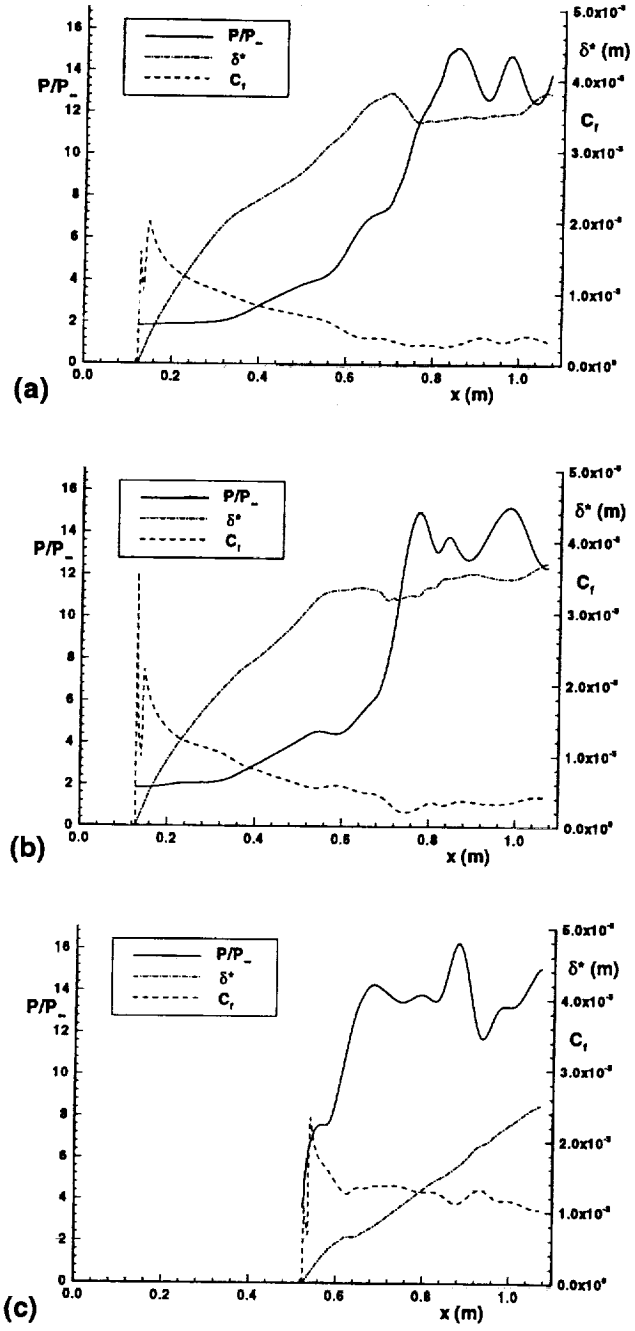

Figure 12. Boundary layer properties along streamlines starting from the midpoints of the top, bottom and side leading edges of the inlet.

Figure 12(a)-(c) show the calculated displacement thickness (δ^*), skin friction (C_f) and imposed pressure distribution (P_e/P_∞) along three streamlines starting from the midpoints of the top, side and bottom leading edges. The pressure distributions in Figs. 12(a) and (b) climb steadily until the throat region, where both jump quickly to a level approximately equal to that at the inlet exit. Displacement thickness on these top and side surface streamlines initially grows quite quickly, due in part to the convergence of streamlines. Interestingly, this growth halts at the throat, dips slightly, then continues at a slow rate over the remaining inlet length. The sudden change in the δ^* growth observed at the throat is due to both the rapid pressure rise and cessation of streamline convergence that occurs in this region. The skin friction distributions along these top and bottom surface streamlines are of similar form to that which occurs on a flat plate. However, the extremely low value of C_f reached at the exit of the inlet ($C_f \approx 0.0004$) is a consequence of the substantial streamline convergence that has occurred along their lengths. Generally speaking, streamline convergence leads to a larger δ^* and a reduced C_f relative to a flat plate under the same pressure distribution. The pressure level on the bottom surface streamline (Fig. 12(c)) begins at a much higher value than on the other two streamlines, and rises quickly to the level exiting the inlet. The region over which streamline convergence occurs is also concentrated just downstream of cowl closure. These factors lead to almost linear δ^* growth along this streamline and a C_f distribution with shape and exit value similar to a flat plate under the same conditions.

Smoothed δ^* distributions calculated along 36 streamlines starting at the top, side and bottom leading edges were added to the inviscid shape of the inlet to obtain its viscous corrected shape. The cross-sections of the resultant inlet are shown in Fig. 13. No boundary layer calculations were instigated at the inlet corners, so the coordinates corresponding to the "corners" of each cross-section were calculated by extrapolation from adjacent points. Only subtle differences between the inviscid and viscous corrected shapes were apparent, however the overall contraction ratio of the inlet has reduced to $CRT_{VIS} = 4.67$, with an internal contraction ratio of $CRI_{VIS} = 2.12$.

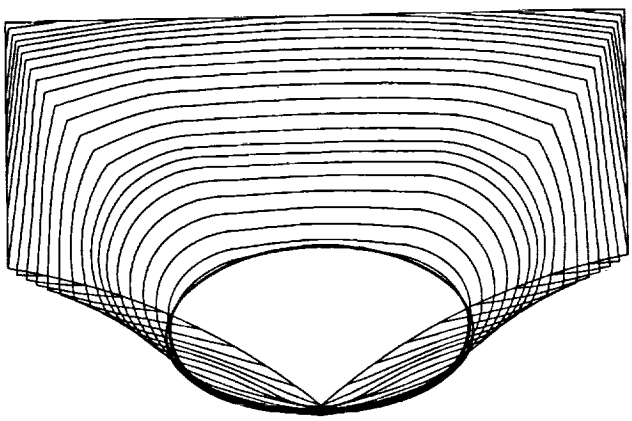

Figure 13. Cross-section shape distributions of the viscous corrected inlet.

With the completion of the viscous correction a more realistic estimate of the inlet performance parameters may be made. The flow exiting the inlet consists of approximately 60% boundary layer by area. Equivalent one-dimensional mass flow weighted performance parameters obtained by combining the boundary layer and core flows of the REST inlet are P_R = 0.458, η_{KE} = 0.975 and η_{KD} = 0.899. Note that the estimated total pressure recovery for the actual inlet is significantly reduced from its inviscid level of P_R = 0.854, as are the estimates of η_{KE} and η_{KD}. These performance levels, while lower than the inviscid values, correspond to those of a very efficient inlet at Mach 7.1. Figure 14 shows a comparison of the REST inlet performance with some mass flow weighted P_R values from a number of wind tunnel tests of three-dimensional inlets reported in Refs. 1,3 and 6. Also included in Fig. 14 is the equivalent one-dimensional P_R value for a Mach 8.33 Busemann inlet tested by Molder et al.[17] in a gun tunnel. While comparison of inlets with different contraction ratio's, mass capture percentages and design Mach numbers is somewhat arbitrary, Fig. 14 does indicate that REST inlets designed using the current procedure promise

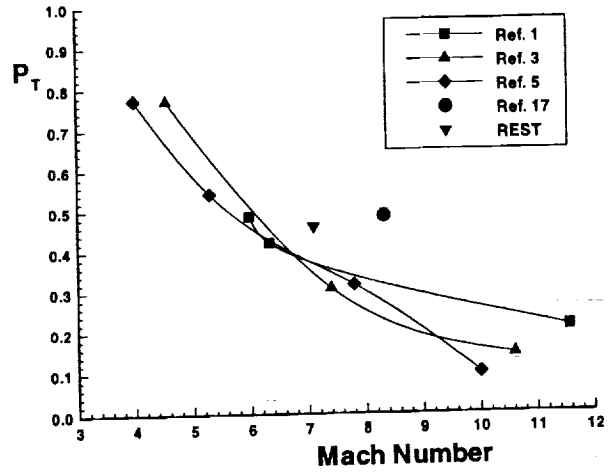

Figure 14. Performance comparison of hypersonic inlets.

higher inlet performance than similar fixed geometry configurations designed and tested in the 1960's. This superior performance is thought to be mainly due to the inclusion of the three-dimensional boundary layer correction in the design procedure, and to a lesser extent on the optimization of the inlet shape transition afforded by the three-dimensional CFD. Neither of these steps were included in the design of the inlets described in Refs. 1-3 and 6. The Busemann inlet tested by Molder et al.[17], which included a viscous correction as part of its design, exhibits the best performance of all the inlets included in the Fig. 14. This inlet requires some form of variable geometry to enable starting, and is included to give some appreciation for the performance penalty paid for the utility of a fixed geometry inlet.

Conclusions

A methodology was presented for the design of three-dimensional hypersonic inlets with rectangular to elliptical shape transition. These fixed geometry inlets included highly swept leading edges and a significantly notched cowl to allow self-starting at ramjet/scramjet take-over speeds. The inviscid portion of the design procedure made extensive use of streamtracing methods and a mathematical lofting technique to determine an aerodynamically efficient shape transition. Furthermore, the surface pressure signature of the inlet flowfield was compared with established correlations to check for shock induced boundary layer separation. The final step in the procedure involved a simplified three-dimensional turbulent boundary layer calculation for determination of the physical inlet shape which generates the desired inviscid flowfield. This design procedure utilized currently available computational tools and high speed computers to perform the numerous cycles needed to complete a design.

The characteristics of a Mach 7.1 inlet designed with the current methodology were described. Inviscid flowfield calculations indicated that this inlet exhibited good on-design performance while generating a relatively uniform exit flow. This was considered to be a significant achievement given its substantial shape transition. Examination of the off-design inviscid performance down to Mach 4.0 indicated an increased level of exit flow non-uniformity and a minimum mass capture of 84.4%. However its performance remained above that of an optimized two-dimensional inlet down to Mach 4.0. Completion of the viscous correction allowed performance estimates of P_R = 0.458, η_{KE} = 0.975 and η_{KD} = 0.899 for the actual inlet. If realized in practice, these levels correspond to a highly efficient inlet for scramjet applications. This work clearly shows the performance advantages that may be gained through the use of three-dimensional inlet geometries relative to more traditional inlet configurations designed using two-dimensional techniques.

References

[1]Hartill, W.B., "Analytical and experimental

investigation of a scramjet inlet of quadriform shape", Tech Rep. AFAPL-TR-65-74, U.S. Airforce, August 1965, Marquardt Corporation.

[2]Keirsey, J.L. and Snow, M.L., "Modular inlet investigation ", Quarterly Report AQR/66-1, Aeronautics Division, Research and Development, Applied Physics Laboratory, Johns Hopkins University, January-March, 1966.

[3]Kutshenreuter, P.H., "Hypersonic inlet tests in helium and air", General Electric Company Advanced Engine and Technology Departments, Cincinnati, Ohio; presented at the AIAA Propulsion Joint Specialist Conference, The Unites States Air Force Academy, Colorado, June 14-18, 1965.

[4]Kantrowitz, A. and Donaldson, C., "Preliminary investigation of supersonic diffusers", NACA ACR No. L5D20, 1945.

[5]Simmons, J.M. and Weidner, E.H., "Design of scramjet inlets with rectangular to circular shape transition", NASA TM No. 87752, June 1986.

[6]Billig, F.S., "Supersonic Combustion Ramjet Missile", Journal of Propulsion and Power, Vol. 11, No. 6, pp 1139-1146, 1995.

[7]Smart, M.K., "Calculation of streamtraced hypersonic inlet performance on and off design", paper No. 5330, 21st International Symposium on Shock Waves, Great Keppel, Australia, July 1997.

[8]Salas, M.D., "Shock fitted method for complicated two-dimensional supersonic flows", AIAA Journal, vol. 14, No. 5, pp 583-588, 1976.

[9]Amtec Engineering TECPLOT™ version 6 Users Manual, Amtec Engineering Inc, 1993.

[10]Barger, R.L., "A procedure for designing forebodies with constraints on cross-section shape and axial area distribution", NASA TP 1881, 1981.

[11]Korkegi, R.H., "Comparison of shock induced two and three-dimensional incipient turbulent separation", AIAA Journal, Vol. 13, No. 4, pp534-535, 1975.

[12]Aerosoft Inc. GASP version 3 Users Manual, Aerosoft Inc, Blacksburg, Virginia, 1996.

[13]Singh, D.J., Trexler, C.A. and Young, J.A., "Three-dimensional simulation of a translating strut inlet", Journal of Propulsion and Power, Vol. 10, No. 2, pp191-197, 1994.

[14]Cebeci, T. and Bradshaw, P, "Physical and Computational Aspects of Convective Heat Transfer", Springer-Verlag, New York, 1994.

[15]Keller, H.B., "A new difference scheme for parabolic problems"; in Numerical Solution of Partial Differential Equations (J. Bramble, ed.), Vol. 2, Academic, New York, 1970.

[16]Cebeci, T. and Smith, A.M.O., "Analysis of Turbulent Boundary Layers", Academic, New York, 1974.

[17]Molder, S., McGregor, R.J., and Paisley, T.W., "A comparison of three hypersonic inlets"; section 6 of "Investigations in the fluid mechanics of scramjet inlets", U.S. Airforce Report WL-TR-2091, 1993.